Geophys. J. Int. (2007) **169,** 839–848 doi: 10.1111/j.1365-246X.2007.03397.x

Three-dimensional modelling of streaming potential

M. R. Sheffer and D. W. Oldenburg

Department of Earth and Ocean Sciences, University of British Columbia, Vancouver, B.C., V6T 1Z4*, Canada. E-mail: msheffer@eos.ubc.ca*

Accepted 2007 February 8. Received 2006 September 1

SUMMARY

The self-potential (SP) method responds to the electrokinetic phenomenon of streaming potential and has been applied to hydrogeologic and engineering investigations to aid in the evaluation of subsurface hydraulic conditions. To enable the study of variably saturated flow problems of complicated geometry, a 3-D finite volume algorithm is developed to evaluate the SP distribution resulting from subsurface fluid flow. The algorithm explicitly calculates the distribution of streaming current sources and solves for the SP given a model of hydraulic head and prescribed distributions of the streaming current cross-coupling conductivity and electrical conductivity. The forward solution is verified by comparing it with an analytical solution for a point source of flow and measured data taken at the surface of a homogeneous embankment. We apply the forward model to a synthetic pumping well example to illustrate that heterogeneous physical property distributions can result in significant charge accumulation. The sign and magnitude of this secondary charge is determined by the physical property and potential gradients at the interface, and can complicate the interpretation of SP data when a single primary flow source is assumed. The 3-D character of the SP response to seepage through an embankment and foundation is illustrated in a preliminary study of SP data collected at a dam site in British Columbia.

Key words: finite volume, hydrology, numerical modelling, potential field, self-potential, streaming potential.

1 INTRODUCTION

Fluid flow through porous media generates electrical current flow, which can be characterized through a series of electrode measurements to produce a map of potential. This electrokinetic phenomenon of streaming potential is one of several coupled flow mechanisms, such as thermoelectric and electrochemical effects, that can be measured using the self-potential (SP) method.

Streaming potential is the common if not dominant driving mechanism for the SP signal in geothermal exploration (Corwin & Hoover 1979; Ishido & Pritchett 1999), earthquake prediction (Mizutani *et al.* 1976; Corwin & Morrison 1977; Fitterman 1978), groundwater studies (Titov *et al.* 2005a) and engineering and environmental investigations (Bogoslovsky & Ogilvy 1973; Corwin 1990).

Given the analogous behaviour of hydraulic and electrical flow systems and the principles of coupled flow, the SP distribution can be studied to evaluate characteristics of the hydraulic regime. A coupled flow model is required to explain the interaction of the hydraulic and electrical flow systems, and the convection current approach proposed by Sill (1983) has been the elemental theory implemented in most numerical investigations of streaming potential. Wurmstich *et al.* (1991) used a 2-D finite element code to analyze seepage and the streaming potential response in a model embankment. Wurmstich & Morgan (1994) developed a 3-D finite difference algorithm to study streaming potential signals caused by oil well pumping in a fluid-saturated half-space. Ishido & Pritchett (1999) studied the streaming potential response in geothermal reservoir simulations using a finite difference post-processor. Revil *et al.* (1999) used a finite element model to evaluate the streaming potential response over a geothermal field driven by both advective and convective fluid flow. Titov *et al.* (2002, 2005b) developed a 2-D finite difference program to evaluate streaming potential responses in groundwater flow problems.

In this paper we present a 3-D finite volume algorithm for calculating the SP distribution resulting from fluid flow in a porous medium. The algorithm was developed to enable the study of variably saturated flow problems of complex geometry for application to engineering and hydrogeological investigations. The equations that describe the hydraulic and electrical flow problems are developed in Section 2. Section 3 describes the forward modelling methodology and the finite volume solution for SP. The numerical solution of a simple flow problem is compared with an analytical solution as a means of verifying the algorithm.

A quantitative study of streaming potential relies on realistic estimates of the relevant physical properties. Section 4 discusses the assignment of streaming current cross-coupling conductivity and electrical conductivity distributions for different hydraulic systems. The unconfined flow problem of seepage through a homogeneous embankment is studied as an example. Section 5 develops an equation that describes primary and secondary sources of charge that

contribute to the SP response. An example of a pumping well is used to illustrate how heterogeneous physical property distributions give rise to secondary sources of charge, which can contribute significantly to the SP response.

Finally, a field data example of seepage through an earth embankment and foundation is described in Section 6. This example clearly illustrates the need for 3-D modelling capability to correctly capture the flow regime in a problem of complex geometry.

2 THEORY

2.1 Primary flow

Fluid flow through a fully saturated porous medium is described using the mass conservation equation stated in terms of hydraulic head h[m]:

$$\nabla \cdot \boldsymbol{q} = -S_s \frac{\partial h}{\partial t} + Q\delta(r - r_s)\,, \tag{1}$$

where $\boldsymbol{q}$ is the volumetric flux [$m^3\ s^{-1}\ m^{-2}$], Q is an additional term used to represent any external point sources of fluid flow imposed on the volume [$m^3\ s^{-1}\ m^{-3}$], and r_s denotes the source location. The specific storage of the volume, S_s [$m^3\ m^{-1}\ m^{-3}$] takes the form

$$S_s = \rho_f g(\alpha + n\beta), \tag{2}$$

where ρ_f is fluid density [$kg\,m^{-3}$], α is the compressibility of the solid matrix [$m^3\ Pa^{-1}\ m^{-3}$], β is the fluid compressibility [$m^3\ Pa^{-1}\ m^{-3}$] and g is gravitational acceleration.

Phenomenological laws have been shown empirically to describe irreversible flow as a linear relation between flux and the gradient of a scalar potential. Fluid flux under laminar flow conditions may be described using a form of Darcy's law:

$$\boldsymbol{q} = -K\nabla h, \tag{3}$$

where K is the hydraulic conductivity [$m\,s^{-1}$] of the volume under study.

The conservation of charge equation is used to describe electrical current flow:

$$\nabla \cdot (\rho_e \boldsymbol{v}) = -\frac{\partial \rho_e}{\partial t}, \tag{4}$$

where $\boldsymbol{v}$ is the volumetric flux [$m^3\ s^{-1}\ m^{-2}$] and ρ_e is the volumetric charge density [$C\,m^{-3}$]. The charge flux term $\rho_e \boldsymbol{v}$ may be written instead as a volumetric current density $\boldsymbol{J}$[$A\,m^{-2}$], by considering the definition of electric current. Eq. (4) now takes the form

$$\nabla \cdot \boldsymbol{J} = -\frac{\partial \rho_e}{\partial t} + I\delta(r - r_s), \tag{5}$$

where I [$A\,m^{-3}$] is the current flow of any external source imposed on the volume. Conduction current density is described using Ohm's law:

$$\boldsymbol{J} = -\sigma\nabla\phi, \tag{6}$$

where ϕ [V] is the electrical potential and σ[$S\,m^{-1}$] is the electrical conductivity.

2.2 Coupled flow

The interdependence of fluid, temperature, electrical and chemical flow systems can be defined using the theory of coupled flow, which describes the flux of a given quantity in terms of the sum of primary and secondary gradients. A generalized constitutive relation that includes both primary and coupled flow terms is

$$\boldsymbol{\Gamma}_i = -\sum_{j=i}^{n} L_{ij}\nabla\Phi_j, \tag{7}$$

where $\boldsymbol{\Gamma}_i$ is the flux of the quantity i under study, Φ_j is the scalar potential and L_{ij} is the conductivity term, which is an averaged macroscopic property representative of the volume under study.

The importance of each term on the total flux is dependent on the relative magnitude of the gradient and the corresponding conductivity coefficient such that, for sufficiently slow processes, flow may result from not only the primary gradient, but also from the secondary gradients. In the absence of significant chemical or temperature gradients the coupled flow equations that describe electrokinetic phenomena are

$$\boldsymbol{\Gamma}_f = -L_{ff}\nabla\Phi_f - L_{fe}\nabla\Phi_e, \tag{8a}$$

and

$$\boldsymbol{\Gamma}_e = -L_{ee}\nabla\Phi_e - L_{ef}\nabla\Phi_f. \tag{8b}$$

The cross-coupling conductivity coefficients link the secondary gradients to the primary flow terms such that $L_{fe}\nabla\Phi_e$ describes fluid flow due to electro-osmosis and $L_{ef}\nabla\Phi_f$ describes streaming current flow. These phenomena are connected through the Onsager reciprocal relations that state $L_{fe} = L_{ef}$, provided the flux and gradient terms are formulated properly, and that flow can be adequately represented by linear constitutive equations in a given system (Onsager 1931).

The gradient terms are considered thermodynamic forces and must be formulated to uphold the principles of non-equilibrium thermodynamics (de Groot 1951). Consequently, potential must be expressed in terms of energy per unit quantity i. We define the hydraulic potential Φ_f [$J\,kg^{-1}$ or $m^2\ s^{-2}$], which may be described using Bernoulli's equation and related to hydraulic head through the relation $\Phi_f = gh$. Accordingly, $\Gamma_f = \rho_f \boldsymbol{q}_T$ represents the total mass flux and the primary conductivity term can be defined as $L_{ff} = \rho_f K/g$. Substituting these relations into (8a) gives

$$\rho_f \boldsymbol{q}_T = -\frac{\rho_f K}{g}\nabla gh - L_{fe}\nabla\phi. \tag{9}$$

In a similar fashion, $\Phi_e = \phi$ is the electric potential [$J\,C^{-1}$ or V], $\Gamma_e = \boldsymbol{J}_T$ represents the total charge flux [$C\,s^{-1}\ m^{-2}$ or $A\,m^{-2}$] and $L_{ee} = \sigma$ is the electrical conductivity. Eq. (8b) now becomes

$$\boldsymbol{J}_T = -\sigma\nabla\phi - L_{ef}\nabla gh. \tag{10}$$

The cross-coupling coefficients L_{fe} and L_{ef} in (9) and (10) are equal and have units of [$A\,s^2\ m^{-3}$]. Re-arranging terms simplifies the equations to

$$\boldsymbol{q}_T = -K\nabla h - k_e\nabla\phi, \tag{11a}$$

and

$$\boldsymbol{J}_T = -\sigma\nabla\phi - L\nabla h, \tag{11b}$$

where $k_e = L_{fe}/\rho_f$ is the coefficient of electro-osmotic permeability [$m^2\ s^{-1}\ V^{-1}$] and $L = gL_{ef}$ is the streaming current cross-coupling conductivity coefficient [$A\,m^{-2}$].

2.3 Governing equations

The constitutive relations defined in (11) are now combined with the continuity equations to define the hydraulic and electrical flow problems.

In the study of streaming potentials, the hydraulic gradient is the driving force and the second term in (11a) can be neglected. This is supported by Mitchell (1991), who reported negligible contribution of the electro-osmotic flow term in materials with $K > 10^{-9}\,\mathrm{m\,s^{-1}}$. We recognize this uncoupled flow equation as a form of Darcy's law, which is combined with (1) to define the saturated hydraulic flow equation:

$$\nabla \cdot K \nabla h = S_s \frac{\partial h}{\partial t} - Q\delta(r - r_s). \tag{12}$$

Variably saturated flow problems require the use of both (12) and an unsaturated flow equation, such as

$$\nabla \cdot K(S_w)\nabla h = n \frac{\partial S_w}{\partial t} - Q\delta(r - r_s), \tag{13}$$

where K is now a function of fluid saturation S_w. Steady-state or transient forms of the fluid flow equation may be used to solve the hydraulic problem, depending on the temporal nature of the boundary conditions.

Once we have solved the hydraulic problem for the distribution of hydraulic head h, the subsequent problem is to solve for the SP distribution. Since hydraulic relaxation times are orders of magnitude larger than electrical relaxation times, electrical conduction current flow is treated as a steady-state process regardless of the nature of the hydraulic process. This suggests that 'snapshots' of the fluid flow regime over time may be analysed as a dc problem. Substitution of (11b) into the steady-state form of (5) results in the coupled electrical flow equation:

$$\nabla \cdot \sigma \nabla \phi = -\nabla \cdot L \nabla h, \tag{14}$$

when there are no imposed external sources of current flow.

3 FORWARD MODELLING METHODOLOGY

The fluid and electrical flow equations are similar in form and hence one could envisage using the same algorithm (e.g. Wurmstich & Morgan 1994). However, we choose to use established programs to solve the hydraulic problem to facilitate both mixed boundary conditions and model calibration, as well as the solution of variably saturated flow problems.

Fluid flow modelling is performed using the 3-D finite difference codes MODFLOW, developed by the US Geological Survey (Harbaugh *et al.* 2000), for saturated flow and MODFLOW-Surfact (HydroGeoLogic Inc. 2005) for variably saturated flow problems.

The electrical eq. (14) is solved using a finite volume approach and our code is independent of the solution of the hydraulic problem. All that is required is to be able to import values of the hydraulic head. In the following sections we outline the numerical details that pertain to our solution.

3.1 Finite volume solution for self-potential

The flow domain constitutes a 3-D volume, which consists of a homogeneous or heterogeneous earth model and in some cases surface water, as indicated in Fig. 1. We recognize electrical property distributions to be discontinuous at interfaces between different materials in the subsurface (e.g. between units 1 and 2 in Fig. 1), as well as at the earth's surface, where a large conductivity contrast exists. Consequently, we do not wish to evaluate the derivative of σ and instead restate (14) as two first-order equations with unknown variables

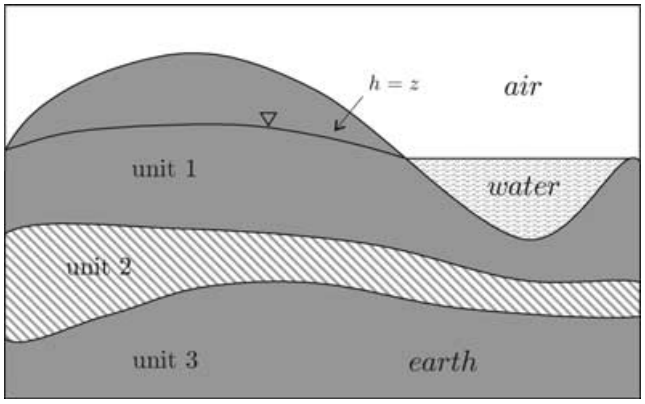

Figure 1. Schematic of the spatial flow domain.

$\boldsymbol{J}$ and ϕ:

$$\nabla \cdot \boldsymbol{J} = f, \tag{15a}$$

and

$$\sigma^{-1}\boldsymbol{J} - \nabla\phi = 0, \tag{15b}$$

where $\boldsymbol{J}$ is the conduction current density. The source term f describes sources of streaming current:

$$f = -\nabla \cdot L \nabla h. \tag{15c}$$

The differential eqs (15a) and (15b) are expressed in their weak forms and discretized using a finite volume method (Haber *et al.* 2000). The chosen arrangement of (15b) is a consequence of the fact that while $\boldsymbol{J}$ is a continuous function, σ and $\nabla\phi$ are discontinuous across an interface separating regions of different conductivity. Integrating these discontinuous variables separately adds accuracy to the solution for ϕ.

The study region is represented by a rectilinear mesh of grid cells. The discrete equations are solved on a staggered grid, with normal components of $\boldsymbol{J}$ located at cell faces and values of potential located at cell centres, as shown in Fig. 2. Each grid cell is assigned an electrical conductivity σ and a cross-coupling conductivity L. These properties are treated as a constant for each cell, but are considered to be piecewise constant in the domain and can vary significantly from one cell to the next.

The equations in (15) must be supplied with boundary conditions. In our implementation we define the outer surface of the domain $\partial\Omega$ as a Neumann no-flow boundary:

$$\boldsymbol{J} \cdot \hat{n}|_{\partial\Omega} = 0. \tag{16}$$

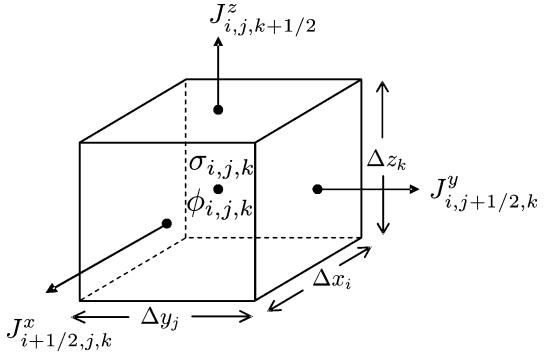

Figure 2. Single grid cell showing cell dimensions, location of components of current density $\boldsymbol{J}$ at cell faces, and location of potential ϕ and conductivity σ at the cell centre.

This condition requires that the outer edge of the domain be positioned far from convective sources to remove the influence of the boundary on the solution in the region of interest. To achieve this, the mesh is expanded beyond the physical extents of the study region by successively increasing cell dimensions in each direction.

The electrical conductivity and cross-coupling conductivity models are defined on the expanded mesh, which is generally much larger than the volume studied in hydraulic modelling. The cross-coupling coefficients in this expanded region are set to zero, but a serious effort should be made to estimate reasonable values of electrical conductivity. A more detailed treatment of electrical property models is given in Section 4.

Applying the finite volume technique to the equations in (15) yields the discrete system:

$$\mathbf{DSG}\phi = -\mathbf{DLGh}, \tag{17}$$

where matrix **D** is the divergence operator, **G** is the gradient operator and the physical property matrices **S** and **L**, respectively, contain the harmonic averages of electrical conductivity σ and cross-coupling coefficient L. Vectors ϕ and **h**, respectively, contain values of electrical potential and hydraulic head. The no-flow boundary condition in (16) is imposed by the divergence matrix **D**. Eq. (17) represents a non-unique solution for ϕ. This non-uniqueness is removed by specifying a constant value of ϕ at a single corner of the grid.

The matrix system in (17) is solved using the biconjugate gradient stabilized method (BiCGSTAB) (Van der Vorst 1992) with preconditioning (Barrett *et al.* 1994). For preconditioning we use either symmetric successive over relaxation (SSOR) or incomplete LU (ILU).

Once (17) has been solved, potential or potential difference data are evaluated as:

$$\mathbf{d} = \mathbf{Q}\phi, \tag{18}$$

where matrix **Q** performs a tri-linear interpolation of ϕ using the eight nearest cell values. In a practical SP survey configuration, data are potential differences that are acquired with respect to a reference electrode. The reference electrode can be located at an arbitrary coordinate in the grid.

3.2 Example: Injection well in a homogeneous half-space

A single point source of fluid flow in a homogeneous, saturated half-space is a straightforward flow problem that is useful to illustrate the SP response to a primary source of streaming current, and to verify the numerical algorithm against an analytical solution.

The hydraulic problem represents an injection well that is screened over a finite portion of its length, as illustrated in Fig. 3. The semi-infinite homogeneous half-space was modelled as a single isotropic geologic unit 500-m-thick extending 10 km in both

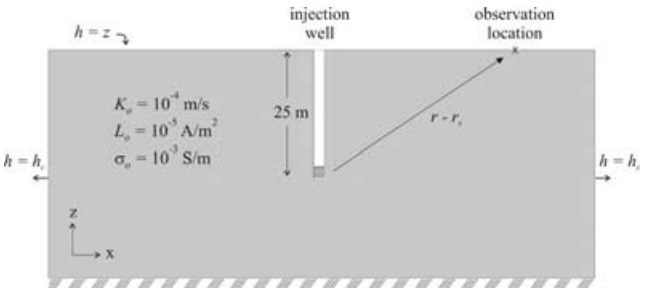

Figure 3. Homogeneous half-space model with injection well showing hydraulic boundary conditions and physical properties of aquifer.

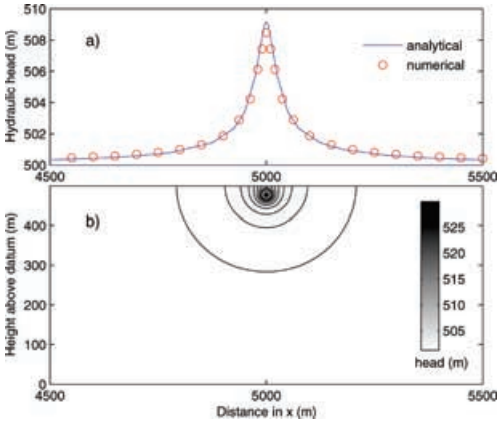

Figure 4. Hydraulic head distribution resulting from a point injection well in a homogeneous half-space: (a) analytical and numerical solutions at surface and (b) predicted head contours (1 m interval).

x- and y-directions. Half-space properties are $K_o = 1 \times 10^{-4}$ m s^{-1}, $L_o = 1 \times 10^{-5}$ A m^{-2}, and $\sigma_o = 1 \times 10^{-3}$ S m^{-1}. The well screen is centred at a depth of 25 m, and fluid is injected at a constant flow rate of 10 000 m^3 day^{-1}.

3.2.1 Numerical solution

Hydraulic head was resolved on a 190 × 190 × 35 non-uniform mesh. Cell lengths in the x and y directions ranged from 3.3 m at the centre of the mesh to 100 m at the edges. Cell heights ranged from 3.3 m at the well screen to 20 m at depth. A constant head boundary of 500 m was defined at the x and y limits of the mesh. This discretization was chosen to facilitate an accurate solution of head in the vicinity of the well. The SP distribution was resolved on a 212 × 212 × 52 mesh in which cell size was progressively expanded by a factor of 1.3. Potential data are referenced to a surface point at the edge of the study region, 5 km from the well. Fig. 4 shows the predicted hydraulic head distribution in the xz plane of the well. Results are presented as a surface profile in Fig. 4(a), and in cross-section in Fig. 4(b). Similarly, the predicted SP distribution is presented in Fig. 5. Although they are of opposite polarity, a strong similarity is evident between the SP and head equipotential distributions.

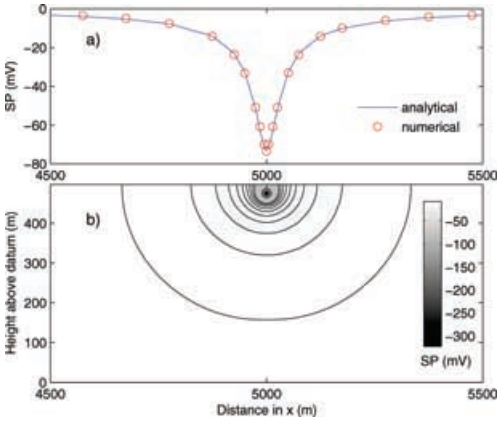

Figure 5. SP distribution resulting from a point injection well in a homogeneous half-space: (a) analytical and numerical solutions at surface and (b) predicted SP contours (5 mV interval).

3.2.2 Analytical solution

To facilitate an analytical solution the equations governing hydraulic and electrical flow are stated as Poisson's equations. The hydraulic equation that defines this problem is the steady-state form of (12):

$$\nabla^2 h = -\frac{1}{K} Q\delta(r - r_s). \tag{19}$$

Similarly, substitution of (19) into (14) reduces the electrical flow equation to:

$$\nabla^2 \phi = \frac{L}{\sigma K} Q\delta(r - r_s). \tag{20}$$

The method of images is used to solve the problem analytically, to account for perturbations in the potential fields caused by the presence of the ground surface. When observations are made at surface, the solutions to (19) and (20) reduce to:

$$h(x, y, 500) = -\frac{Q(r_s)\, v_s}{2\pi K |r - r_s|}, \tag{21}$$

and

$$\phi(x, y, 500) = \frac{L\, Q(r_s)\, v_s}{2\pi \sigma K |r - r_s|}, \tag{22}$$

respectively, where v_s represents the source volume and $|r - r_s|$ denotes the distance between the source and observation location. The analytical solutions for h and ϕ at the ground surface show excellent agreement with the numerical results, as illustrated in the profile plots of Figs 4 and 5.

4 PHYSICAL PROPERTIES

4.1 The cross-coupling conductivity coefficient

By applying the divergence theorem, the coupled electrical flow eq. (14) can be expressed as

$$\int_s \sigma \nabla\phi \cdot d\mathbf{s} = -\int_s L \nabla h \cdot d\mathbf{s}. \tag{23}$$

In a homogeneous medium,

$$\sigma \int_s \nabla\phi \cdot \hat{n}\, ds = -L \int_s \nabla h \cdot \hat{n}\, ds, \tag{24}$$

where L and σ are macroscopic properties. If we consider a 1-D flow experiment in a porous medium of length Δx and cross-sectional area A, in which flow occurs along the length of the medium, (24) is evaluated to give

$$\sigma \frac{\Delta\phi}{\Delta x} A = -L \frac{\Delta h}{\Delta x} A. \tag{25}$$

Eq. (25) may be further simplified and rearranged to define the cross-coupling conductivity:

$$L = -\sigma C, \tag{26}$$

where

$$C = \frac{\Delta\phi}{\Delta h}. \tag{27}$$

The streaming potential coupling coefficient C, which is often reported in terms of fluid pressure, may be characterized through laboratory measurements and is typically a negative quantity (e.g. Ishido & Mizutani 1981; Morgan *et al.* 1989; Jouniaux & Pozzi 1995; Pengra *et al.* 1999). The above definition of C is consistent with our formulation of the coupled flow equations in terms of hydraulic head, as shown in (11).

4.2 Defining σ and L property distributions

Representative values of the cross-coupling conductivity and electrical conductivity must be prescribed for all porous media in the model domain, and can be assigned using measured or theoretical estimates. Electrical conductivity can be measured in the field or laboratory using geophysical techniques such as the dc resistivity method, or estimated in certain cases using an empirical relation such as Archie's Law (Archie 1942), which can be adjusted to account for varying degrees of saturation (e.g. Bear 1972). The streaming potential coupling coefficient can be measured in the laboratory as noted in the section above, or estimated using a form of the Helmholtz–Smoluchowski equation (Overbeek 1952), which shows that C is a function of fluid conductivity. Since both σ and C vary with the electrical conductivity of the saturating fluid, appropriate corresponding values must be used to calculate L using (26).

As illustrated in Fig. 1, the flow domain comprises an earth model and may also include surface water. The earth model can consist of a number of distinct units, where each unit is characterized by representative values of L and σ. Since streaming current flow is limited only to porous media, air and water bodies are assigned a null cross-coupling conductivity to impose a no-flow boundary at the physical limits of the porous medium. However, surface water is assigned representative values of fluid conductivity σ_f to permit conduction current flow. Air is typically assigned an electrical conductivity $\sigma_{\text{air}} = 1 \times 10^{-8}$ S m^{-1}.

In a confined fluid flow problem, the earth model under study is in a completely saturated state. Consequently, saturated material properties are used to describe each unit, i.e. $L = L^{\text{sat}}$ and $\sigma = \sigma^{\text{sat}}$. In an unconfined fluid flow problem, a phreatic surface delineates the boundary between saturated and unsaturated zones. The position of this boundary is defined where pore fluid pressure is atmospheric (i.e. $h = z$), as indicated in Fig. 1. If the phreatic surface intersects a given earth model unit, representative properties must be assigned to both saturated and unsaturated zones within the unit.

There are two approaches to determining a hydraulic solution to an unconfined flow problem. In a saturated or free-surface approach, fluid flow is assumed to dominate below the phreatic surface and is not considered in the unsaturated zone. The position of the phreatic surface, and consequently the size of the saturated model domain, is not known *a-priori* and is determined through the hydraulic flow analysis. In a variably saturated approach, fluid flow is evaluated within both the saturated and unsaturated zones. This latter approach generates a more realistic hydraulic solution in problems with steeply dipping interfaces, and is necessary for transient simulations (Freeze 1971). The delineation between saturated and unsaturated zones is determined by the condition $h = z$.

The behaviour of streaming current flow in the unsaturated zone is not addressed here. For simplicity, we consider streaming current flow to be limited to the saturated zone, such that the phreatic surface acts as a no-flow boundary. This condition is imposed by specifying $L^{\text{unsat}} = 0$. However, the conduction current permeates both saturated and unsaturated zones, and a representative σ^{unsat} is chosen to reflect the unsaturated or partially saturated conditions of the material. For simplicity, we assume a constant value of σ^{unsat} for each unit, which does not vary with the decline in saturation above the phreatic surface. The next example illustrates the assignment of physical properties in an unconfined flow problem.

4.3 Example: Homogeneous lab-scale embankment

The SP response to steady-state seepage through a laboratory-scale embankment is examined as an example of an unconfined flow

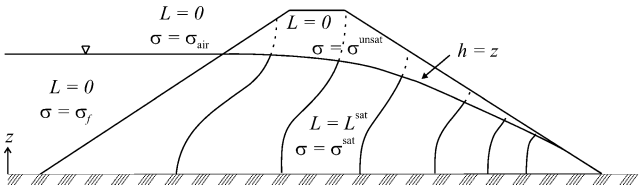

Figure 6. Schematic cross-section of a homogeneous earth embankment, illustrating the distribution of electrical properties. Hydraulic head equipotential lines are indicated in the figure, with dotted lines representing hydraulic head in the unsaturated zone. Superscripts *sat* and *unsat* refer to representative properties of the saturated and unsaturated zones, respectively. The value σ_f represents the electrical conductivity of the impounded water. The value σ_{air} is typically chosen as 1×10^{-8} S m^{-1}.

problem, and provides a means of verifying the SP algorithm with measured data.

The homogeneous embankment under study was constructed of Ottawa sand in an acrylic tank and measures 140 cm in length, 10 cm in width and 31 cm in height. The dam was subjected to steady-state flow from constant reservoir heights of 18 and 22.5 cm. The hydraulic conductivity and electrical properties of the sand were derived from laboratory testing and are represented in the model as: $K = 4.5 \times 10^{-4}$ m s^{-1}, $L^{\text{sat}} = 2.5 \times 10^{-4}$ A m^{-2}, $\sigma^{\text{sat}} = 2.5 \times 10^{-3}$ S m^{-1} and $\sigma^{\text{unsat}} = 1.5 \times 10^{-3}$ S m^{-1}. The electrical conductivity of the reservoir water σ_f was measured as 2.8×10^{-3} S m^{-1}. Fig. 6 illustrates a schematic of the electrical property distribution in the study region.

The embankment was modelled using a $70 \times 5 \times 16$ mesh with a uniform cell dimension of 2 cm. The SP distribution was resolved on a padded grid, in which padding cells were assigned an electrical conductivity of 1×10^{-8} S m^{-1} to represent air. The predicted hydraulic head distribution and SP response at the surface of the embankment are shown for each reservoir level in Figs 7 and 8. The SP data are referenced to a point centred at the surface of the crest. Predicted and measured SP data at each reservoir level are compared in Figs 7(a) and 8(a) and show good agreement. The increase in SP amplitude with reservoir level is a direct consequence of the increase in hydraulic gradient across the embankment.

The chosen L and σ property distributions influence how electrical current flows in the subsurface. Fig. 9 displays fluid, streaming current and conduction current flux patterns for the 22.5 cm reservoir model described in Fig. 8. Fig. 9(a) shows vectors of fluid flux $\boldsymbol{q}$ within the saturated zone below the phreatic surface. Fig. 9(b) displays streaming current flow, which is limited to the saturated

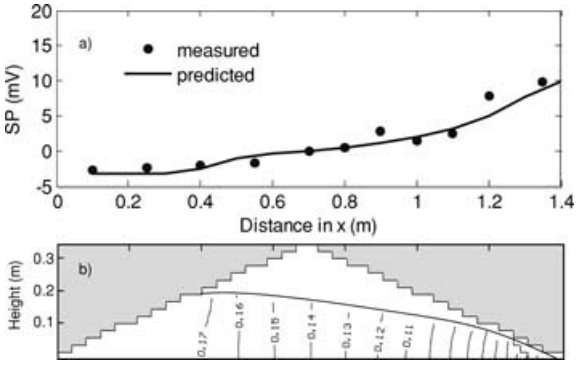

Figure 7. Homogeneous embankment subject to steady-state seepage from an 18 cm reservoir: (a) Measured and predicted SP data at surface and (b) predicted hydraulic head distribution (m).

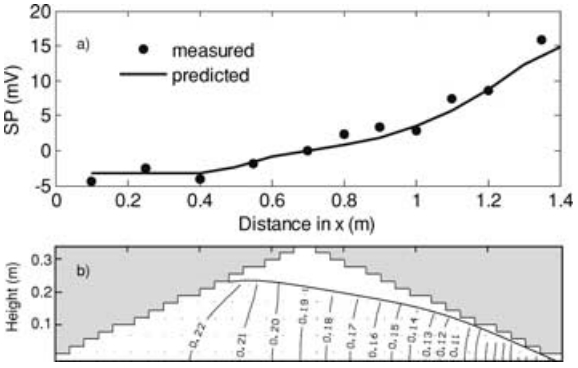

Figure 8. Homogeneous embankment subject to steady-state seepage from a 22.5 cm reservoir: (a) Measured and predicted SP data at surface and (b) predicted hydraulic head distribution (m).

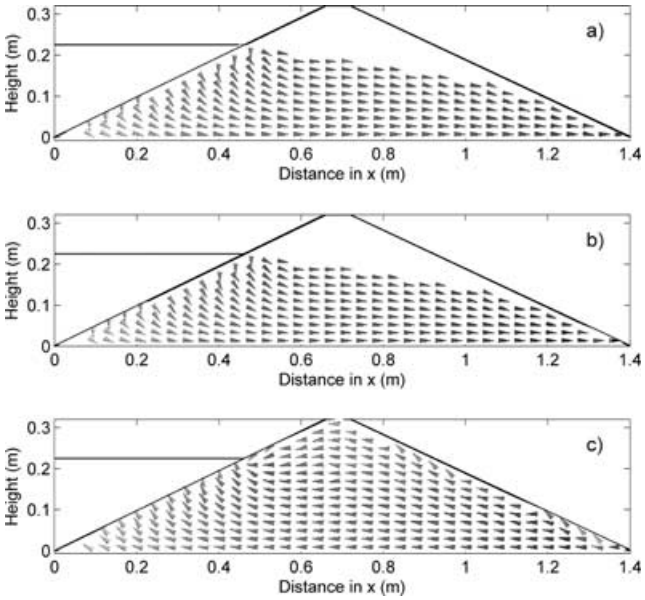

Figure 9. Homogeneous embankment subject to steady-state seepage from a 22.5 cm reservoir: (a) fluid flux $\boldsymbol{q}$; (b) streaming current and (c) conduction current $\boldsymbol{J}$.

zone since the electrical problem is solved using a saturated flow assumption ($L^{\text{unsat}} = 0$). Streaming current and fluid flow vector fields appear very similar since both processes are driven by hydraulic gradients in the saturated zone. Fig. 9(c) illustrates vectors of conduction current flow $\boldsymbol{J}$, which is not confined to the saturated zone and is governed by the electrical conductivity distribution.

5 SOURCES OF CHARGE CONTRIBUTING TO THE SELF-POTENTIAL

Conduction current flow and the corresponding SP field is governed by the distribution of streaming current sources and electrical conductivity in the subsurface. To enable an intuitive understanding of the potential response, (14) is expressed as a Poisson equation and restated in terms of charge density. This equation clearly defines the physical conditions that dictate the magnitude and sign of current sources in the subsurface. All properties are assumed isotropic for the sake of discussion.

The source function f defined in (15) describes all sources of streaming current in the study region. The nature of these convective sources may be examined by expanding (15a) to:

$$\nabla \cdot \boldsymbol{J} = -L\nabla^2 h - \nabla L \cdot \nabla h. \tag{28}$$

The steady-state form of (12) is expanded and re-arranged to give:

$$\nabla^2 h = -\frac{1}{K} Q\delta(r - r_s) - \frac{1}{K} \nabla K \cdot \nabla h. \tag{29}$$

Substitution of (29) into (28) results in:

$$\nabla \cdot \boldsymbol{J} = \frac{L}{K} Q\delta(r - r_s) + \frac{L}{K} \nabla K \cdot \nabla h - \nabla L \cdot \nabla h. \tag{30}$$

Here we see an explicit definition of streaming current sources, which may be grouped into two distinct types: (1) 'primary' sources due to the injection or withdrawal of fluid from the system, as described by the fluid flow source term Q and (2) 'secondary' sources that are generated by gradients in the physical properties K and L in the presence of a hydraulic gradient.

Heterogeneities in σ will perturb the potential field generated by the streaming current source distribution, such that boundaries between regions of different σ may also be considered as secondary sources. Invoking Ohm's law, (30) is expanded and re-stated as Poisson's equation for potential ϕ:

$$\nabla^2\phi = \frac{L}{\sigma K} Q\delta(r - r_s) + \frac{L}{\sigma K} \nabla K \cdot \nabla h - \frac{1}{\sigma} \nabla L \cdot \nabla h - \frac{1}{\sigma} \nabla\sigma \cdot \nabla\phi, \tag{31}$$

where the right-hand side is the source function that describes all sources that contribute to ϕ. Finally, (31) is expressed in terms of volumetric charge density ρ_e [C m^{-3}] using Gauss' law:

$$\rho_e = \epsilon_o \left\{ -\frac{L}{\sigma K} Q\delta(r - r_s) - \frac{L}{\sigma K} \nabla K \cdot \nabla h + \frac{1}{\sigma} \nabla L \cdot \nabla h + \frac{1}{\sigma} \nabla\sigma \cdot \nabla\phi \right\}. \tag{32}$$

The SP ϕ is the sum of all potential fields generated by primary and secondary sources of charge within the system, according to the superposition principle. The potential decays with the inverse radial distance $|r - r_s|$ from each source of charge defined by $\rho_e(r_s)$, which may be evaluated through the integral solution:

$$\phi(r) = \frac{1}{4\pi\epsilon_o} \int_V \frac{\rho_e(r_s)}{|r - r_s|} dV. \tag{33}$$

Eqs (32) and (33) provide a basis for an intuitive understanding of the distribution of electrical charge in the subsurface, and the resulting potential response. The first term on the right-hand side of (32) describes primary sources of charge. Primary sources typically manifest as injection or pumping wells in an aquifer. As was illustrated in the example shown in Section 3.2, a positive injection of fluid into the system results in a concentration of negative charge and consequently a negative SP response. The magnitude of this primary source is controlled by the fluid flow rate Q and conductivity values at the source.

The remaining three terms on the right-hand side of (32) describe the secondary sources generated between regions of different conductivity. These are the only sources that contribute to the SP in systems where no primary flow sources exist, such as the earth dam example of Section 4.3. In a discontinuous conductivity model of the earth, secondary sources appear at an interface between different materials or between different saturation states within a given material. The sign of the accumulated charge depends on the sign of the conductivity and potential gradients at the interface.

Transient hydraulic conditions can give rise to a variable charge distribution, which can be evaluated through (32) using time-dependent variables. The release of water from storage in a transient saturated hydraulic analysis manifests as changes in the hydraulic head field with time. Since the conduction current responds instantaneously to hydraulic conditions, as discussed in Section 2.3, the charge distribution and corresponding SP reflects the head distribution at a given point in time. Similarly, transient fluid saturation resulting from a variably saturated flow analysis can give rise to sources of charge, which manifest as changes in the hydraulic head and physical property distributions with time.

In any analysis, the magnitude of secondary charge can be significant and can cause difficulty when the SP interpretation is done in terms of a primary source only. The following example illustrates this.

5.1 Example: Pumping well in a heterogeneous half-space

A pumping well model is used to illustrate the effect of heterogeneous physical property distributions on the SP response to a primary flow source. This example serves to show that a heterogeneous hydraulic conductivity distribution can greatly influence the character of the SP distribution, whose magnitude is influenced by the electrical properties of the subsurface.

Fig. 10 displays a schematic of the heterogeneous half-space model, which represents a pervious sand lens buried within a silty sand deposit. The chosen hydraulic conductivity and electrical properties of the sand aquifer are $K = 1 \times 10^{-4}$ m s^{-1}, $L^{\text{sat}} = 3 \times 10^{-5}$ A m^{-2} and $\sigma^{\text{sat}} = 2 \times 10^{-3}$ S m^{-1}. The silty sand half-space properties are $K = 1 \times 10^{-6}$ m s^{-1}, $L^{\text{sat}} = 1 \times 10^{-5}$ A m^{-2} and $\sigma^{\text{sat}} = 5 \times 10^{-3}$ S m^{-1}. In this example we assume $\sigma^{\text{unsat}} = \sigma^{\text{sat}}$ for simplicity. The well penetrates the sand aquifer

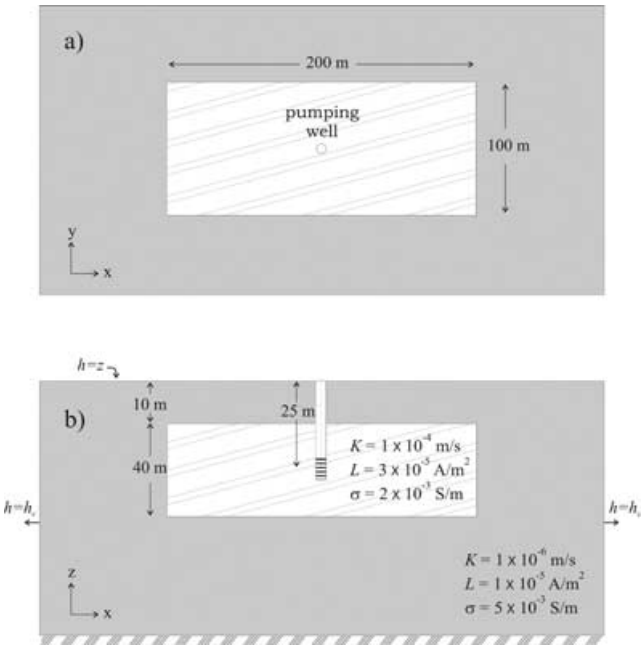

Figure 10. Heterogeneous half-space with pumping well: (a) model in plan view, showing outline of subsurface aquifer; (b) model in cross-section, showing hydraulic boundary conditions and physical properties of aquifer and half-space. Well screen length is 10 m.

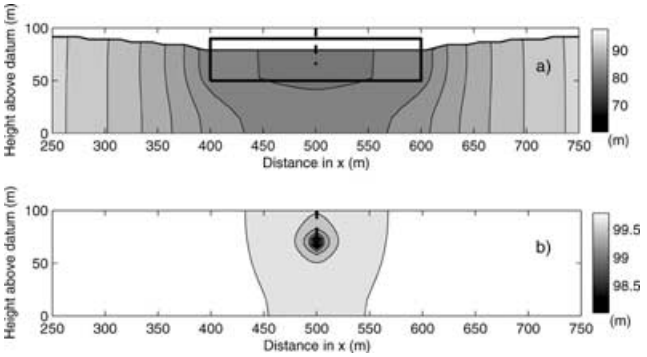

Figure 11. Vertical cross-section of hydraulic head in the plane of the pumping well: (a) heterogeneous half-space model; (b) homogeneous half-space ($K = 1 \times 10^{-4}$ m s^{-1}) for comparison.

and is pumped at a constant rate of 500 m^3 day^{-1}. Steady-state hydraulic conditions are simulated and the water table is assumed to be at ground surface a distance from the well. The study region was modelled using a non-uniform 99 × 99 × 22 cell mesh, extending 100 m in depth and 1000 m in x and y directions. The pumping rate is averaged over the total volume of the two grid cells used to represent the well screen, such that the pumping rate per unit volume is 1.3×10^{-5} m^3 s^{-1} m^{-3}.

Fig. 11 illustrates the hydraulic head contours in a vertical xz plane centred on the well. Since the confined sand aquifer is more permeable to fluid flow relative to the silty sand half-space, water is drawn into the aquifer from the surrounding medium. Pumping causes a drawdown in the water table to a height of 78 m at the well, as shown in Fig. 11(a). Fig. 11(b) shows the hydraulic head contours for the same pumping well in a homogeneous aquifer ($K = 1 \times 10^{-4}$ m s^{-1}) for comparison. Although the well is pumped at the same rate, there is no drawdown in the water table.

The chosen pumping rate and physical property distributions dictate the sign and magnitude of streaming current sources in the subsurface. Fig. 12(a) shows the primary source associated with the pumping well in a homogeneous half-space model of the aquifer. The pumping well equates to a primary source of positive charge. The total magnitude of this primary current source is equal to 7.8×10^{-6} A m^{-3} (3.9×10^{-6} A m^{-3} in each grid cell representing the well screen), which is consistent with that predicted using the

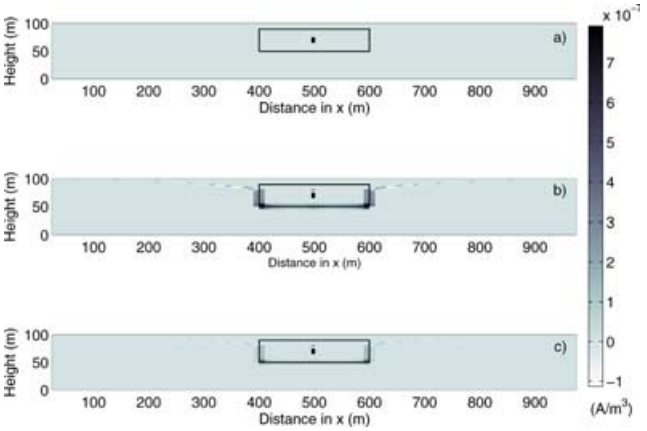

Figure 12. Vertical cross-section of streaming current source density in the plane of the pumping well: (a) homogeneous half-space; (b) heterogeneous K half-space and (c) heterogeneous K and L half-space. The total magnitude of primary streaming current sources at the well screen is 7.8×10^{-6} A m^{-3}.

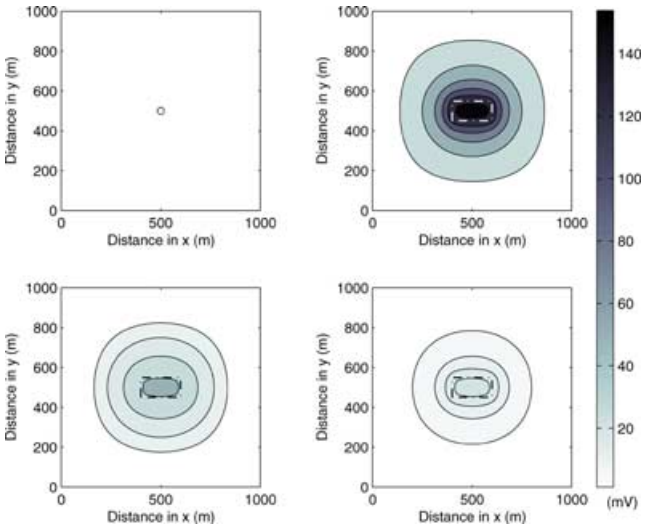

Figure 13. Surface plan map of SP: (a) homogeneous half-space; (b) heterogeneous K half-space; (c) heterogeneous K and L half-space and (d) heterogeneous K, L and σ half-space.

first term of (30). The corresponding SP distribution at surface is shown in Fig. 13(a), which shows a positive SP anomaly centred on the well.

The relative influence of each secondary source term is examined by progressively increasing the level of heterogeneity in the model. The chosen heterogeneous hydraulic conductivity distribution causes positive charge to accumulate at the interface between the aquifer and surrounding half-space, as shown in Fig. 12(b). This model assumes that K varies but that L and σ of the half-space are equal to that of the aquifer. The secondary sources are of smaller magnitude than the primary source, but collectively they contribute significantly to the SP response at the ground surface, as shown in Fig. 13(b). Here we see that the SP contour pattern roughly delineates the shape of the aquifer. Introducing a heterogeneous L distribution in addition to the heterogeneous K model decreases the magnitude of the secondary streaming current sources, as indicated in Fig. 12(c), since the chosen L values result in the accumulation of negative charge at the interface. However, the net SP response remains positive, as shown in Fig. 13(c). The chosen heterogeneous distribution of σ results in a further decrease in the magnitude of secondary sources at the aquifer interface, as illustrated by the surface SP pattern shown in Fig. 13(d). Fig. 14 illustrates the surface SP data in profile form, along a line at $y = 500$ m. The secondary sources caused by heterogeneous K, L and σ distributions result in a SP signature of much different amplitude and shape to that predicted using a homogeneous half-space model.

6 FIELD EXAMPLE

One of the principle motivations for undertaking this research is the interpretation of SP data collected during embankment dam seepage investigations. Flow through an embankment and foundation is a problem of complicated geometry that requires a 3-D model to properly characterize the hydraulic head and corresponding SP distributions across the structure.

SP surveys were performed at a dam site in British Columbia to aid in the assessment of overall seepage conditions, and to investigate the integrity of certain components of the site, which are discussed below. The surveys took place in 2001 May and August

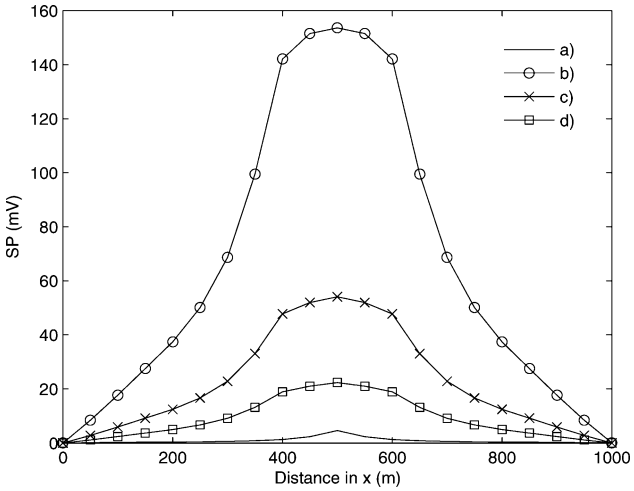

Figure 14. Surface profiles of SP at $y = 500$ m: (a) homogeneous half-space; (b) heterogeneous K half-space; (c) heterogeneous K and L half-space and (d) heterogeneous K, L and σ half-space.

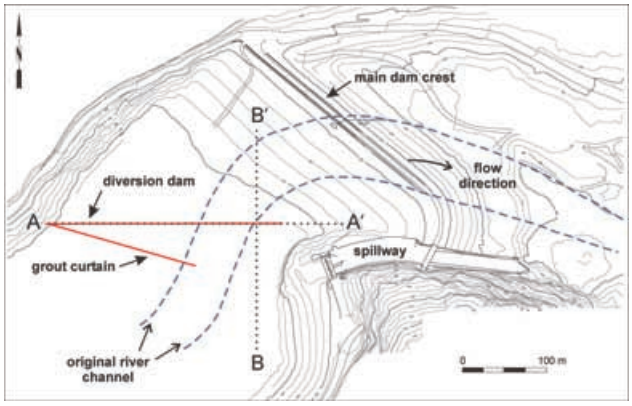

Figure 15. Plan map of the embankment dam site, indicating key structural features and survey lines A-A′ and B-B′.

respectively, to capture representative high and low pool conditions. Data were collected over the surface of the embankment and reservoir using $CuSO_4$ electrodes with a fixed-base electrode configuration, and were corrected for telluric variations. Preliminary modelling was undertaken to aid in the interpretation of SP data collected at the site. Our goal was to generate a preliminary 3-D simulation of the SP distribution using best estimates of the physical properties K, L and σ.

The key features of the site are highlighted in the plan map shown in Fig. 15 and a conductivity model shown in Fig. 16. The main dam is a zoned earthfill dam, which is underlain by alluvial deposits and situated within a granite bedrock valley. A pre-existing diversion dam is located at the upstream toe of this main dam. A clay blanket lines the upstream face of the main dam and keys into the central impervious core of the diversion dam. The foundation materials consist of pervious upper and lower aquifers, which are separated by a thick clay layer. A sheet-pile cut-off wall coincides with the crest of the diversion dam and extends vertically through the upper aquifer into the clay layer to prevent seepage through this zone. A deep grout cut-off is located further upstream and controls seepage through the lower aquifer. The clay blanket, diversion dam core, sheet-pile cut-off and grout curtain form a continuous impervious barrier to flow through the dam and foundation.

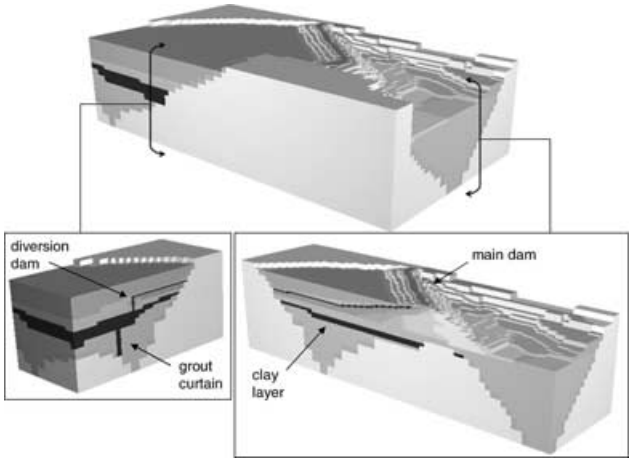

Figure 16. Model of the embankment dam and foundation.

Fourteen distinct soil and geologic units are defined in the model of the site. Values of K, L and σ were assigned to each zone in the model. Hydraulic conductivity values were derived from published estimates (Terzaghi & Lacroix 1964). Values of cross-coupling conductivity and electrical conductivity were assigned based on published and theoretical estimates for typical soil and rock types found at site, using average reservoir water conductivity values measured during the course of SP surveys performed at the site. These physical property distributions were assigned as a first approximation, and all units were each represented by uniform property distributions.

Fig. 17 compares measured and predicted data taken along two perpendicular lines at the surface of the reservoir corresponding to the high pool survey. Fig. 17(a) shows data along the diversion dam crest, and Fig. 17(b) shows data in a N–S direction across the grout curtain. Measured and predicted data compare well, and show general agreement of trends and range of amplitude. This gives us confidence in both the modelling results and our initial

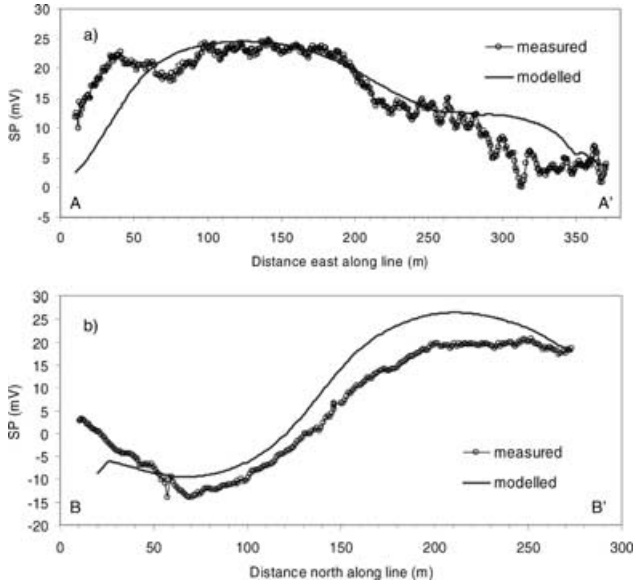

Figure 17. Embankment subject to seepage from the reservoir at high pool: (a) Measured and predicted SP data at the surface of the reservoir above the diversion dam (survey line A-A′) and (b) Measured and predicted SP data at the surface of the reservoir in a N–S direction across the grout curtain (survey line B-B′).

estimates of the physical property distributions. The data clearly show the 3-D nature of the SP distribution at the site. Effective interpretation will require further work and the development of an inverse methodology.

7 CONCLUSION

We have developed a 3-D forward modelling algorithm that calculates the SP field induced by fluid flow in the subsurface, based on the theory of coupled flow. The algorithm was developed using a finite volume discretization on a staggered grid, and explicitly calculates all streaming current sources based on known distributions of hydraulic head and physical properties, namely the streaming current cross-coupling conductivity and electrical conductivity.

The algorithm was used to successfully reproduce an analytical point source solution and approximate the measured SP response to seepage through a homogeneous earth dam. A synthetic pumping well example illustrated that heterogeneous physical property distributions result in an accumulation of charge at physical boundaries. The sign and magnitude of this charge is determined by the physical property and potential gradients at the boundary, and can contribute significantly to the SP signal resulting from a primary source. Preliminary modelling of the SP response to seepage at an embankment dam site illustrated the need for a 3-D model to characterize the SP distribution at a complicated site. These four examples clearly demonstrate the link between the SP and hydraulic head distributions. This suggests that information about the hydraulic system may be inferred from the SP data, given some knowledge of the electrical property distribution in the subsurface.

ACKNOWLEDGMENTS

The work presented here was sponsored by the Canadian Electrical Association Technologies, Inc. Dam Safety Interest Group, and funded in part by the Natural Sciences and Engineering Research Council of Canada. We are grateful for their support. We thank Eldad Haber and Roman Shekhtman for their significant contributions to the development of the numerical code. We also extend thanks to British Columbia Hydro and Powertech Labs, Inc. for releasing the field and laboratory data sets.

REFERENCES

Archie, G.E., 1942. The electrical resistivity log as an aid in determining some reservoir characteristics, *Transactions of the Society of Petroleum Engineers of the American Institute of Mining, Metallurgical and Petroleum Engineers (AIME),* **146,** 54–67.

Barrett, R. et al., 1994. *Templates for the Solution of Linear Systems: Building Blocks for Iterative Methods*, Society for Industrial and Applied Mathematics (SIAM), Philadelphia.

Bear, J., 1972. *Dynamics of Fluids in Porous Media,* Dover Publications, Inc., New York.

Bogoslovsky, V.V. & Ogilvy, A.A., 1973. Deformations of natural electric fields near drainage structures, *Geophys. Prospect.,* **21,** 716–723.

Corwin, R.F., 1990. The self-potential method for environmental and engineering applications, *in Geotechnical and Environmental Geophysics,* Vol. 1, pp. 127–145, ed. Ward, S.H., Society of Exploration Geophysicists, Tulsa.

Corwin, R.F. & Hoover, D.B., 1979. The self-potential method in geothermal exploration, *Geophysics,* **44**(2), 226–245.

Corwin, R.F. & Morrison, H.F., 1977. Self-potential variations preceding earthquakes in central California, *Geophys. Res. Lett.,* **4,** 171–174.

de Groot, S.R., 1951. *Thermodynamics of irreversible processes,* Vol.3 of Selected Topics in Modern Physics, North Holland Publishing Company, Amsterdam.

Fitterman, D.V., 1978. Electrokinetic and magnetic anomalies associated with dilatant regions in a layered earth, *J. geophys. Res.,* **83**(B12), 5923–5928.

Freeze, R.A., 1971. Influence of the unsaturated flow domain on seepage through earth dams, *Water Resources Research,* **7**(4), 929–941.

Haber, E., Ascher, U.M., Aruliah, D.A. & Oldenburg, D.W., 2000. Fast simulation of 3D electromagnetic problems using potentials, *Journal of Computational Physics,* **163**(1), 150–171.

Harbaugh, A.W., Banta, E.R., Hill, M.C. & McDonald, M.G., 2000. *MODFLOW-2000, The U.S. Geological Survey Modular Ground-Water Model - User Guide to Modularization Concepts and the Ground-Water Flow Process,* Open-File Report 00-92, U.S. Geological Survey, Washington.

HydroGeoLogic, Inc., 2005. *MODFLOW-SURFACT Version 2.2 Documentation,* HydroGeoLogic, Inc., Herndon.

Ishido, T. & Mizutani, H., 1981. Experimental and theoretical basis of electrokinetic phenomena in rock-water systems and its application to geophysics, *J. geophys. Res.,* **86**(B3), 1763–1775.

Ishido, T. & Pritchett, J.W., 1999. Numerical simulation of electrokinetic potentials associated with subsurface fluid flow, *J. geophys. Res.,* **104**(B7), 15 247–15 259.

Jouniaux, L. & Pozzi, J.-P., 1995. Streaming potential and permeability of saturated sandstones under triaxial stress: consequences for electrotelluric anomalies prior to earthquakes, *J. geophys. Res.,* **100**(B6), 10 197–10 209.

Mitchell, J.K., 1991. Conduction phenomena: from theory to geotechnical practice, *Geotechnique,* **43**(3), 299–340.

Mizutani, H., Ishido, T., Yokokura, T. & Ohnishi, S., 1976. Electrokinetic phenomena associated with earthquakes, *Geophys. Res. Lett.,* **3,** 365–368.

Morgan, F.D., Williams, E.R. & Madden, T.R., 1989. Streaming potential properties of Westerly granite with applications, *J. geophys. Res.,* **94**(B9), 12 449–12 461.

Onsager, L., 1931. Reciprocal relations in irreversible processes, I, *Physical Review,* **37,** 405–426.

Overbeek, J.T.G., 1952. Electrokinetic phenomena, in *Colloid Science,* Vol. 1, ed. Kruyt, H.R., Irreversible Systems, Elsevier Publishing Company, Amsterdam.

Pengra, D.B., Li, S.X. & Wong, P., 1999. Determination of rock properties by low-frequency ac electrokinetics, *J. geophys. Res.,* **104**(B12), 29 485–29 508.

Revil, A., Schwaeger, H., Cathles, L.M. III, & Manhardt, P.D., 1999. Streaming potential in porous media 2. Theory and application to geothermal systems, *J. geophys. Res.,* **104**(B9), 20 033–20 048.

Sill, W.R., 1983. Self-potential modeling from primary flows, *Geophysics,* **48**(1), 76–86.

Terzaghi, K. & Lacroix, Y., 1964. Mission dam: an earth and rockfill dam on a highly compressible foundation, *Geotechnique,* **14**(1), 14–50.

Titov, K., Ilyin, Y., Konosavski, P. & Levitski, A., 2002. Electrokinetic spontaneous polarization in porous media: petrophysics and numerical modelling, *Journal of Hydrology,* **267,** 207–216.

Titov, K.V., Levitski, A., Konosavski, P.K., Tarasov, A.V., Ilyin, Y.T. & Bues, M.A., 2005a. Combined application of surface geoelectrical methods for groundwater-flow modeling: a case history, *Geophysics,* **70**(5), H21–H31.

Titov, K., Revil, A., Konosavsky, P., Straface, S. & Troisi, S., 2005b. Numerical modelling of self-potential signals associated with a pumping test experiment, *Geophys. J. Int.,* **162,** 641–650.

Van der Vorst, H.A., 1992. BiCGSTAB: A fast and smoothly converging variant of the Bi-CG for the solution of nonsymmetric linear systems, *Journal on Scientific and Statistical Computing,* **13,** 631–644.

Wurmstich, B. & Morgan, F.D., 1994. Modeling of streaming potential responses caused by oil well pumping, *Geophysics,* **59**(1), 46–56.

Wurmstich, B., Morgan, F.D., Merkler, G.-P. & Lytton, R.L., 1991. Finite-element modeling of streaming potentials due to seepage: study of a dam, *Society of Exploration Geophysicists Technical Program Expanded Abstracts,* **10,** 542–544.